Chapter 6

Concurrent Multi-Target Laser Ablation for Making Nano-Composite Films

Abdalla M. Darwish, Sergey S. Sarkisov and Darayas N. Patel

Additional information is available at the end of the chapter

http://dx.doi.org/10.5772/64816

Abstract

New method of using laser ablation for film deposition that can be called as concurrent multi-beam multi-target matrix-assisted pulsed laser evaporation and pulsed laser deposition (MBMT-MAPLE/PLD) is described. Practical MBMT-MAPLE/PLD system built at Dillard University has three separate laser beams, three targets and the remotely controlled plume overlapping mechanism that provides even mixing of the target materials during their deposition on the substrate. The system accommodates MAPLE targets in the form of polymer solutions frozen with flowing liquid nitrogen. The feasibility of the method was demonstrated when it was used for making polymer nano-composite films with two inorganic additives: upconversion fluorescent phosphor $NaYF_4$:Yb^{3+}, Er^{3+} and aluminum-doped ZnO (AZO). Three laser beams, an infrared 1064-nm beam for the MAPLE and two 532-nm beams for the PLD targets, were concurrently used in the process. The fabricated nano-composite films were characterized using X-ray diffraction, scanning electron microscopy (SEM), optical fluorescent spectroscopy, and the measurement of the quantum efficiency (QE) of the upconversion fluorescence. The size of the inorganic nanoparticles varied in the range 10–200 nm. The AZO additive increased QE by 1.6 times. The conclusion was made on the feasibility of MBMT-MAPLE/PLD method for making multi-component nano-composite films for various applications.

Keywords: laser ablation, pulsed laser deposition, matrix-assisted pulsed laser evaporation, polymer nano-composite films

1. Introduction

Pulsed laser deposition (PLD) is a popular application of laser ablation for making thin films. The technology in its variation of the matrix-assisted pulsed laser evaporation (MAPLE) has become a potent way of making polymer and other organic coatings. The chapter will describe a new method of making nano-composite films based on concurrent ablation/evaporation of more than one organic MAPLE and inorganic PLD targets with several laser beams. The advantage is an independent and optimized control of the deposition conditions for each target. The discussion will include the design of the multi-beam multi-target deposition system, examples of the deposited nano-composite films and their properties, the encountered problems/solutions, and the future trends.

For the last three decades, PLD technique has been intensively used for deposition of many kinds of oxides, nitrides, carbides, and metals and for fabrication of thin films including those composed of superconductors, electro-optic $BaTi0_3$, piezoelectric ZnO, electro-conductive TiO_2, rare earth (RE) doped phosphate glasses, etc [1–14]. Those thin films had many deficiencies that had to be addressed before making them suitable for commercial applications. The technique was used by Smith and Turner [2] in 1965 for the preparation of semiconductor and dielectric thin films. They demonstrated the stoichiometry transfer between the target and the deposited film and high deposition rates of about 0.1 nm per pulse. The occurrence of the droplets of the target material on the substrate surface has been observed in [3]. Despite some encouraging results for single-component films, the conventional single-beam single-target PLD technique remains to be poorly suitable for composite films made of the materials of different nature: one of the reasons that a single laser beam cannot be always suitable for a wide spectrum of materials. Further improvement is a new variant of PLD called the concurrent multi-beam multi-target PLD that deposits different materials simultaneously with different laser beams producing overlapping plumes. In case of polymer nano-composite films at least one of the laser beams and the target must be suitable for the process of deposition of the polymer host, such as MAPLE.

In MAPLE, a frozen solution of a polymer in a volatile solvent becomes a laser target [15–54]. The solvent and concentration of the solution are chosen in such a way that first, the polymer dissolves completely and forms a dilute solution free of particulate; second, the main portion of the laser energy is absorbed by the solvent and not by the solute; and third, no photochemical reaction occurs between the solvent and the solute. The interaction between the laser radiation and matter in MAPLE is a photothermal process. The energy of the laser beam absorbed by the solvent is converted to thermal energy that heats the polymer but causes the solvent to vaporize. As the solvent molecules escape into the gas phase, the polymer molecules gain sufficient kinetic energy via collisions with the evaporating solvent molecules and enter the gas phase as well. Selection of the optimal MAPLE conditions (laser energy and wavelength, pulse repetition rate, type of solvent, concentration of the polymer solution, temperature, and background gas and its pressure) can result in the deposition process with no significant degradation of the polymer. The MAPLE deposition is carried on layer-by-layer, while the concentration of the polymer solution in the ablated target remains constant. When a substrate

is positioned directly in the path of the plume, a film starts forming from the evaporated polymer molecules on a substrate placed in the path of the plume. At the same time, the volatile solvent molecules are taken away from the chamber by the vacuum pump. In case of fabrication of polymer nano-composites, MAPLE targets are usually prepared as nano-colloids of the additives of interest in the initial polymer solutions. Combining the components of different nature, such as polymers and inorganic substances, in the same target and ablating them with the same laser beam rarely results in nano-composite films of fair quality. The laser beam energy and wavelength cannot fit all components in the mixture. Also, the proportion of the components in the film is dictated by the target and cannot be altered in the process. The improvements can be expected in the method of concurrent multi-beam and multi-target deposition using MAPLE polymer targets and inorganic PLD targets, each being concurrently ablated by laser beams of different wavelengths [55–64]. The method can be called as multi-beam multi-target MAPLE and PLD or with acronym MBMT-MAPLE/PLD that is described below.

2. Methods and materials

2.1. Multi-beam multi-target MAPLE/PLD system

The design of the MBMT-MAPLE/PLD system (it is a three-beam and three-target variant) is schematically presented in **Figure 1**. Three laser beams of different wavelength evaporate/ablate concurrently three targets made of different materials (organic or inorganic). The laser beams are forced to scan over the targets with oscillating (in X and Y directions) reflectors in order to eliminate pre-mature target erosion and cracking due to laser-induced target ablation in a single spot. The photograph of the 24″ vacuum chamber of the system at Dillard University and one of three laser beam guides is presented in **Figure 2**.

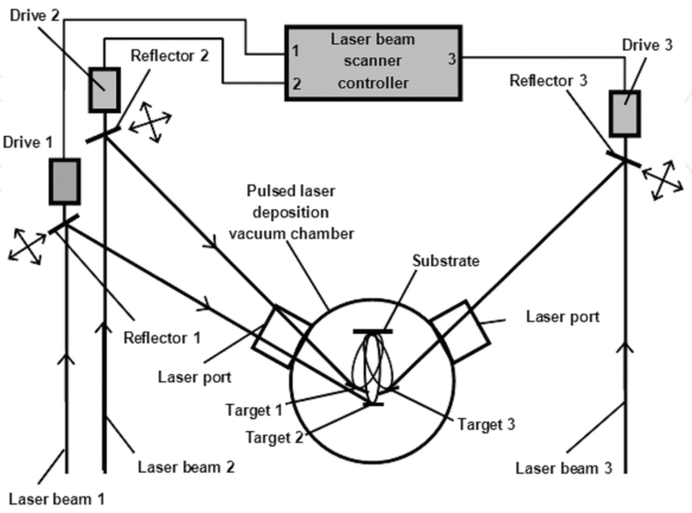

Figure 1. The schematic of the MBMT-MAPLE/PLD system [60].

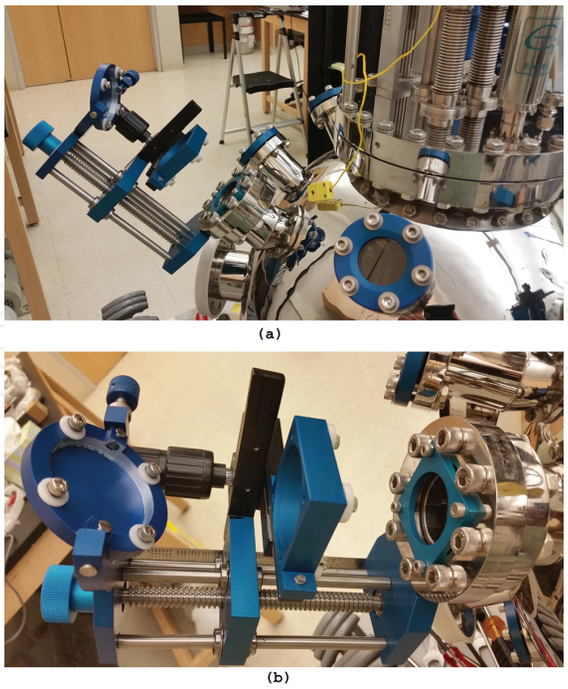

Figure 2. View of the 24″ vacuum chamber of the three-beam MBMT-MAPLE/PLD system at Dillard University (a). The side view of one of the laser beam guides including the holder for the laser beam scanner attached to the optical window of the chamber (b) [60].

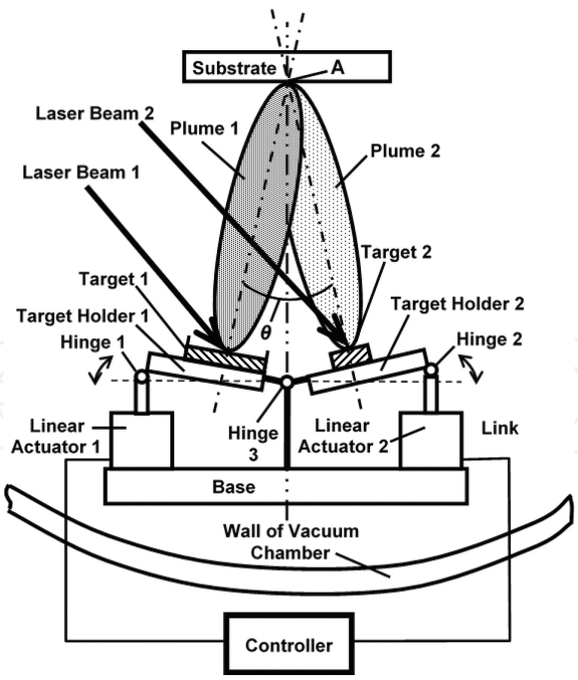

Figure 3. Schematic of the target tilting sub-system of the MBMT-MAPLE/PLD system with remote control of the directions of the plumes. Shown are two targets out of three. θ is the optimal angle between the plums at which they overlap in point A on the surface of the substrate.

http://dx.doi.org/10.5772/64816

The MBMT-MAPLE/PLD system has a sub-system of the plume direction control schematically presented (for two targets for the sake of simplicity) in **Figure 3**. Remotely controlled vacuum compatible linear actuators tilt the targets in order to achieve an optimal angle θ between the plumes (which are perpendicular to the target surfaces) at which the plumes overlap on the surface of the substrate. This secures the uniform mixing of the materials from the targets in the resulting composite film during the deposition process. The photographs of the tilt control sub-system for three targets are presented in **Figure 4**. One important feature of this sub-system is that the target holders are tilted around the axes in the horizontal plane instead of vertical plane, which reduces chances of dropping or spilling the target material.

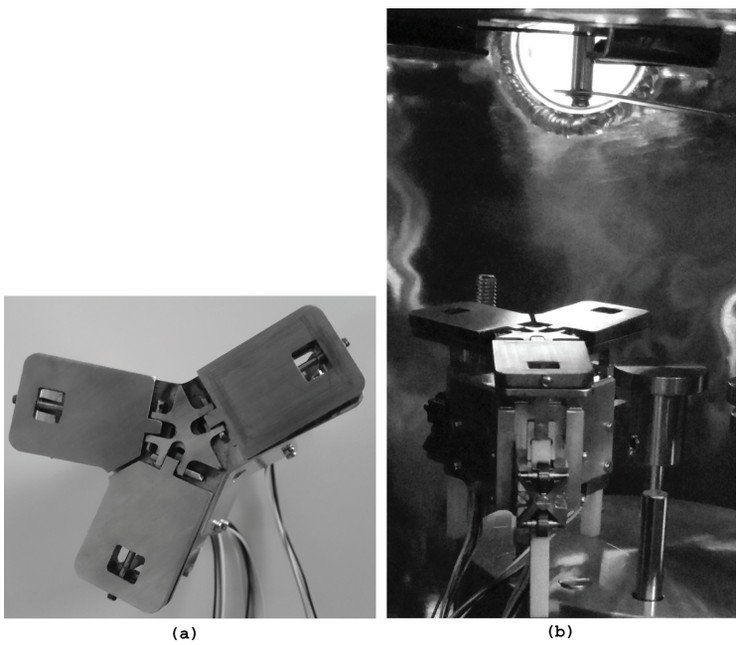

Figure 4. View of the three-target holder with remotely controlled tilt of each target (to achieve overlapping of the plumes on the substrate) (a) and the view of the three-target holder installed inside the vacuum chamber (b).

The target holders of the triple-target sub-system are designed to accommodate MAPLE targets cooled with flowing liquid nitrogen (LN) as presented in **Figure 5**. A copper container for a polymer solution (MAPLE target) is mounted on a copper container for LN (the cooler) that cools the polymer solution (the target) and keeps it frozen. The MAPLE target assembly is connected to the LN feeding and collecting lines (copper tubing) drawn through a flange to be attached to the vacuum chamber. The feeding line is connected to the LN feeding vessel external to the vacuum chamber. The collecting LN line is connected to another external vessel where the LN flows in after passing through the cooler. The MAPLE target assembly is mounted on the top of one of the tilting target holders (**Figure 4**) installed inside the vacuum chamber. Horizontal orientation of the MAPLE target in this design makes possible to conveniently install the empty copper cup in the chamber and fill it later with the liquid polymer solution without the risk of spilling it out before freezing.

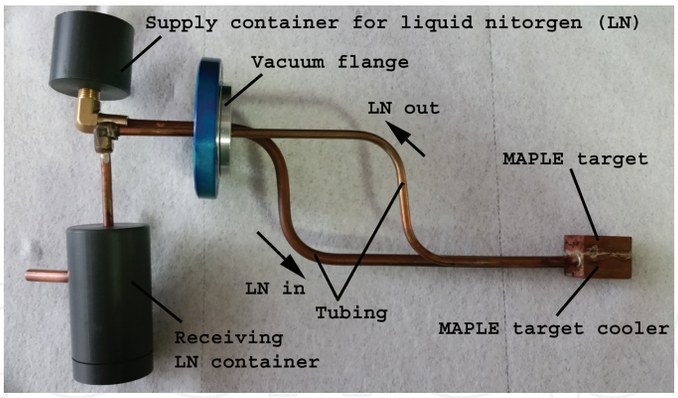

Figure 5. View of the MAPLE target assembly removed from the vacuum chamber. The target is cooled with liquid nitrogen (LN).

2.2. Target materials

The MBPT-MAPLE/PLD method was used to deposit thin films of a polymer nano-composite film with two inorganic additives: upconversion phosphor and the electro-optic enhancer of the upconversion emission.

2.2.1. MAPLE target

The MAPLE target material was the solution of poly(methyl methacrylate) known as PMMA in chlorobenzene at a proportion of 1.0 g solids per 10 mL. The solution was filtered through a 0.2-micron filter.

2.2.2. Inorganic PLD targets

2.2.2.1. Upconversion phosphor

The first inorganic PLD target was made by compressing a powder of efficient upconversion phosphor $NaYF_4$:Yb^{3+}, Er^{3+} with a 25-ton hydraulic press. Upconversion phosphor is a material that absorbs low-energy photons, such as infrared (IR) ones, and re-emits high-energy photons of visible or ultra-violet light. The compounds of the rare earth (RE) elements are particularly attractive as upconversion phosphors with high efficiency of converting IR radiation to upconversion emission. The efficiency depends significantly on the host material for the RE ions. There is a group of efficient upconversion phosphors based on the hexagonal crystalline fluoride $NaYF_4$ (β-$NaYF_4$) as a host. This is due to the low phonon energy of its crystalline lattice that keeps at minimum the rate of the non-radiative multi-phonon relaxation of the excited RE dopant ions. The powder of phosphor $NaYF_4$:Yb^{3+}, Er^{3+} with the doping rates of Yb^{3+} and Er^{3+} 10 and 2%, respectively (10 ytterbium ions and 2 erbium ions per 100 ions of sodium), was synthesized using the wet method [55] and baked for 1 h at 400°C in open air to convert host $NaYF_4$ to its hexagonal crystalline β-phase and maximize the upconversion efficiency. **Figure 6** presents the energy diagram of the phosphor and **Figure 7** its absorption/fluorescence spectra [60]. The energy of the laser photons is mostly absorbed by the ions of

http://dx.doi.org/10.5772/64816

Yb^{3+} acting as synthesizers and then transferred via the energy transfer process to the ions of Er^{3+}, which generated the upconversion, higher energy photons due to the two-photon mechanism. The phosphor powder produced intense visible upconversion emission with two green spectral peaks at 515 and 535 nm and one red spectral peak at 653 nm being pumped with infrared (980 nm) radiation from a laser diode as presented in **Figure 7**. **Figure 8** presents the X-ray diffraction spectrum of the phosphor powder taken with Bruker D2 Phaser X-ray diffractometer. All the observed diffraction peaks can be attributed to β-$NaYF_4$, thus indicating that this is the dominating crystalline phase of the powder.

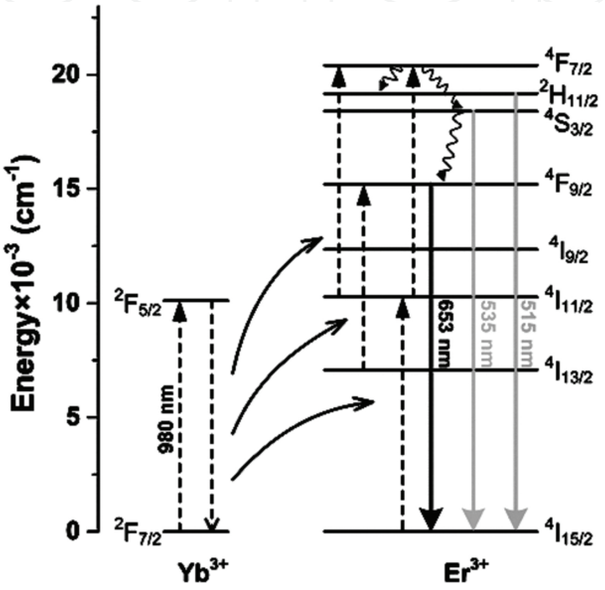

Figure 6. Energy diagram of upconversion phosphor $NaYF_4$: Yb^{3+}, Er^{3+} [60].

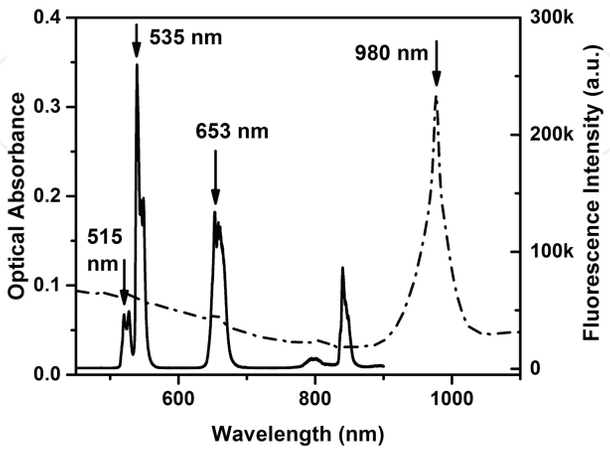

Figure 7. Spectra of optical absorbance (dash-dotted line) and upconversion fluorescence (solid line) of phosphor $NaYF_4$: Yb^{3+}, Er^{3+} [60].

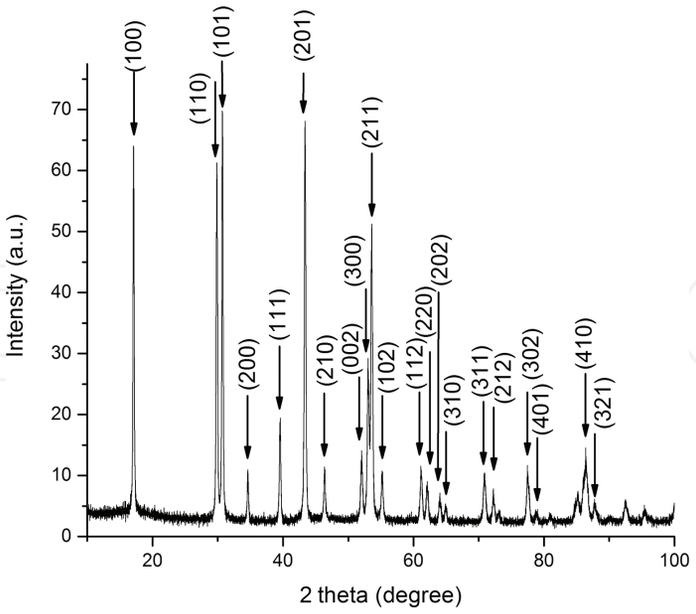

Figure 8. XRD spectrum of the upconversion phosphor powder baked for 1 h at 400°C with the diffraction peaks attributed to the hexagonal β-phase of $NaYF_4$.

2.2.2.2. Electro-optic AZO compound

Aluminum-doped ZnO (AZO) compound is an optically transparent electric conductor with the surface plasmon resonance (SPR) enhancement of local optical field similar to the noble metals, but without significant optical losses attributed to them [65–68]. It can thus be expected that adding AZO nanoparticles to the upconversion phosphor in a polymer nano-composite film will bring the local enhancement of the pumping IR optical field in the vicinity of the phosphor nanoparticles and consequently increase the intensity of the upconversion emission. PLD target was a pellet of $Zn_{0.98}Al_{0.02}O$ where the aluminum fraction was 2% of the total by weight as compared with zinc, not counting the oxygen. The AZO pellet had 20 mm in diameter and 3 mm in thickness. The pellet was prepared by spark plasma sintering (SPS), also referred to as pulsed electric current sintering (PECS). In SPS pulsed DC current passed through a graphite die, as well as the AZO powder compact. Joule heating is the key mechanism in the densification of the powder compact. The densification resulted in near theoretical density at a lower sintering temperature than in conventional sintering. The heat is produced internally. This differs from the regular hot pressing with the heat generated by external source. Due to high heating/cooling rate (up to 1000 K/min) sintering was very fast (within few minutes). High speed of the process ensured it densified the powder without coarsening, which accompanied standard densification routes. While the term "spark plasma sintering" is commonly used, a literal interpretation of the term may be misleading since neither a spark nor a plasma is present in the process. **Figure 9** presents the X-ray diffraction spectrum of the AZO target taken with Bruker D2 Phaser X-ray diffractometer. All the observed diffraction peaks can be attributed to ZnO.

http://dx.doi.org/10.5772/64816

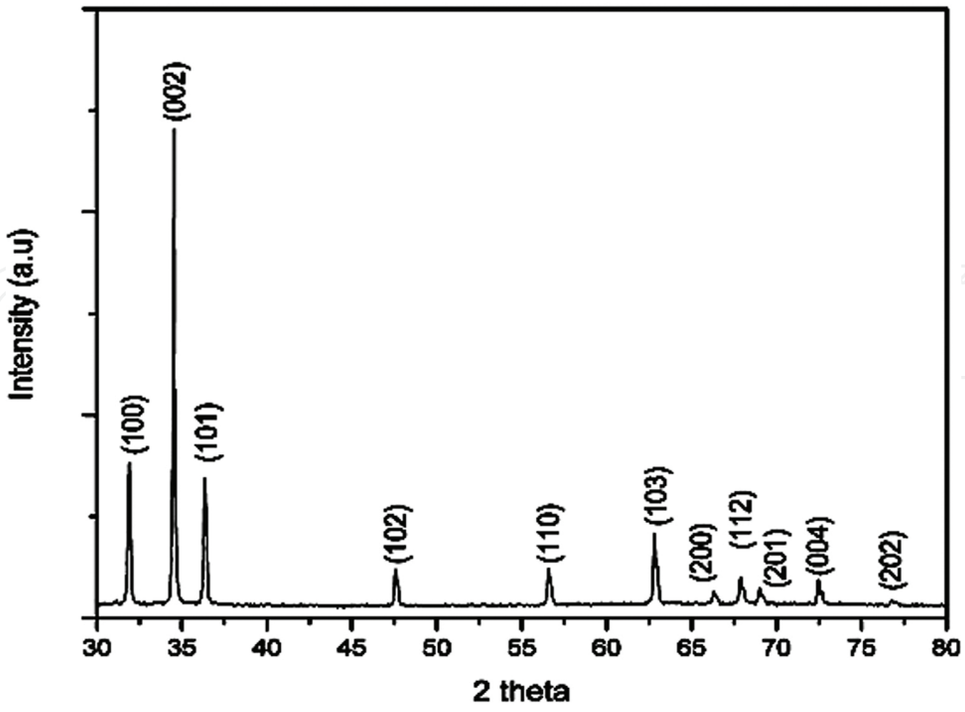

Figure 9. XRD spectrum of the prepared AZO PLD target with the diffraction peaks attributed to ZnO.

2.3. Deposition procedure

The PMMA solution in chlorobenzene was poured in a copper cup of the MAPLE target assembly (**Figure 5**) and frozen with liquid nitrogen. The first PLD target was the pellet of the upconversion phosphor. The AZO pellet was the second PLD target. Two pulsed laser sources were used. The first was a Spectra Physics Quanta Ray Nd:YAG Q-switched Pro-250-50 laser with a pulse repetition rate of 50 Hz, 750-mJ energy per pulse (1064-nm wavelength) and 400-mJ energy per pulse at the 532-nm second harmonic. The second laser source (synchronized with the first laser) was a Spectra Physics Quanta Ray Nd:YAG Q-switched Lab-170-10 laser with a pulse repetition rate of 10 Hz, 850-mJ energy per pulse (1064-nm wavelength) and 450-mJ energy per pulse at the 532-nm second harmonic. The MAPLE target was evaporated with the 1064-nm beam from the first laser source and exposed to the fluence ranging from 0.84 to 2.4 J/cm^2 per pulse. The first PLD target was concurrently ablated with the 532-nm frequency doubled Nd:YAG beam from the same source. The fluence was tuned up between 0.8 and 1.0 J/cm^2 to keep the proportion of the upconversion material in the polymer film at approximately 5% by weight. The second PLD target was concurrently ablated with the 532-nm frequency doubled Nd:YAG beam from the second source. The fluence was tuned up between 1.0 and 2.2 J/cm^2 to keep the proportion of the upconversion material in the polymer film at approximately 5% by weight. The polymer films were deposited on preoxidized Si (100) substrates with a SiO_2 layer thickness of 2.0 μm. The deposition time was ~3.0 min (until PLD targets started showing the signs of erosion). The thickness of the deposited films was between 180 and 200 nm as measured with an atomic force microscope.

3. Properties of the deposited films

3.1. Crystalline structure of the inorganic additives in the polymer nano-composite film

In order to conduct X-ray diffraction spectroscopy, the deposited films were separated from the substrates and placed in a Bruker D2 Phaser X-ray diffractometer. A reference sample of the PMMA nano-composite film containing only one upconversion phosphor additive was also made. The X-ray diffraction spectrum of this sample is presented in **Figure 10**. The spectrum has all the signatures of the hexagonal β-phase $NaYF_4$ that was initially present in the first PLD target made of the upconversion phosphor. **Figure 11** shows the X-ray diffraction spectrum of the polymer nano-composite film including nanoparticles of both inorganic additives: the upconversion phosphor and AZO. The observed spectral peaks include those that can be attributed to both β-phase $NaYF_4$ and AZO. It thus can be concluded that the two inorganic additives have been transferred to the polymer film without modification of their crystalline structure during the PLD process.

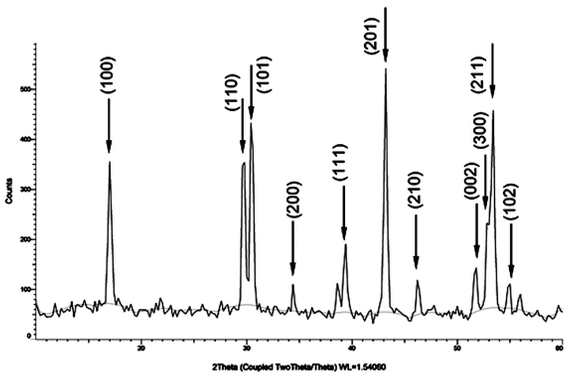

Figure 10. XRD spectrum of the two-component composite film made of PMMA and the nanoparticles of $NaYF_4$: Yb^{3+}, Er^{3+} with the diffraction peaks attributed to the hexagonal β-phase of $NaYF_4$.

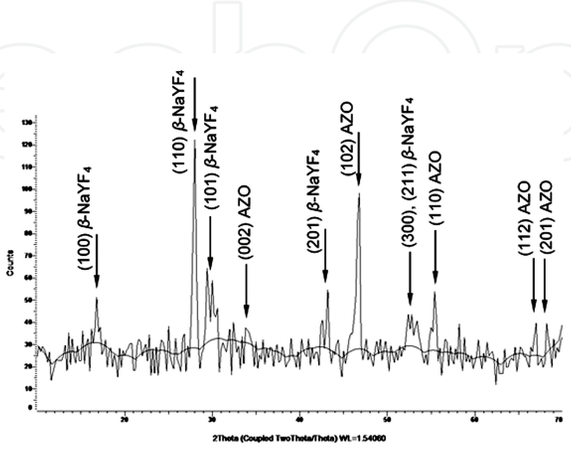

Figure 11. XRD spectrum of the three-component composite film made of PMMA and the nanoparticles of $NaYF_4$: Yb^{3+}, $Er^{3+}$and AZO.

http://dx.doi.org/10.5772/64816

3.2. Morphology

Figure 12 presents the high-resolution scanning electron microscope (SEM) image of the produced nano-composite film with a magnification of ×60 K. For the sake of convenience, the images of some exemplary nanoparticles are marked with arrows. The size of the nanoparticles varied widely in the range of the order of 10–200 nm. The nearly uniform distribution of the nanoparticles in the polymer film was occasionally disrupted by much larger particles or clusters (limited resolution of SEM prohibited distinguishing between large particles and the clusters of nanoparticles) of the order of 500–1000 nm.

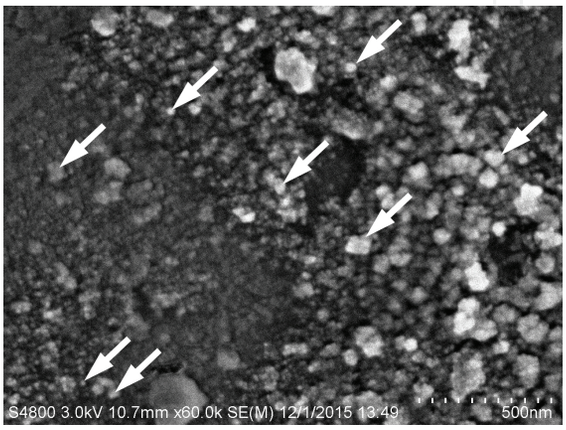

Figure 12. Scanning electron microscopy (SEM) image of the three-component composite film made of PMMA and the nanoparticles of $NaYF_4$: Yb^{3+}, $Er^{3+}$and AZO taken with magnification ×60,000. White arrows point to exemplary nanoparticles of various sizes (from ~10 to 200 nm) embedded in the polymer matrix.

3.3. Fluorescence

The deposited nano-composite films demonstrated visible upconversion fluorescence being pumped with a 980-nm IR radiation from a laser diode (PL980P330J from Thorlabs; 330-mW maximum power; quantum well laser chip, pigtailed with a wavelength stabilizing fiber Bragg grating). The spectrum of the upconversion emission was measured with a Princeton Instruments 500-mm focal-length Spectra Pro (SP–2500i) imaging spectrometer/monochromator equipped with 1200 gr/mm (blazed at 500 nm) holographic diffraction grating. The spectrum presented in **Figure 13** had peaks at 522, 540, and 656 nm and resembled the spectrum of the bulk phosphor target (**Figure 7**).

The upconversion fluorescence of the films was quantitatively characterized by the quantum efficiency (QE) η. QE is the ratio of the number of the photons of the upconversion radiation generated per unit of time n_{up} to the number of the photons of the infrared pump radiation $\eta = (n_{up}/n_{pump}) \times 100\%$ [69]. The quantum efficiencies of green (at 522- and 540-nm spectral peaks combined) upconversion emission of the deposited three-component films (PMMA-phosphor-AZO), two-component films (PMMA-phosphor), and the bulk phosphor target were measured to be of 0.072, 0.045, and 0.56% respectively. QE of the bulk phosphor PLD target compared well against the highest 3% quantum efficiency reported for similar

upconversion phosphor $NaYF_4$: Yb^{3+}, Er^{3+} in the literature [69]. QE of the polymer nano-composite film containing only the nanoparticles of the upconversion phosphor was ~12 times less than that of the bulk phosphor. On the other side, the nano-composite film deposited under similar conditions, but also containing AZO nanoparticles, had QE ~1.6 times greater. This could be attributed to the plasmonic enhancement effect of the AZO nanoparticles on the local optical pump IR field. Since the upconversion emission is a two-photon process, QE could be increased proportional to approximately square of the pump power. In this experiment, the maximum pump power was limited to 150 mW, less than the damage threshold of the nano-composite film.

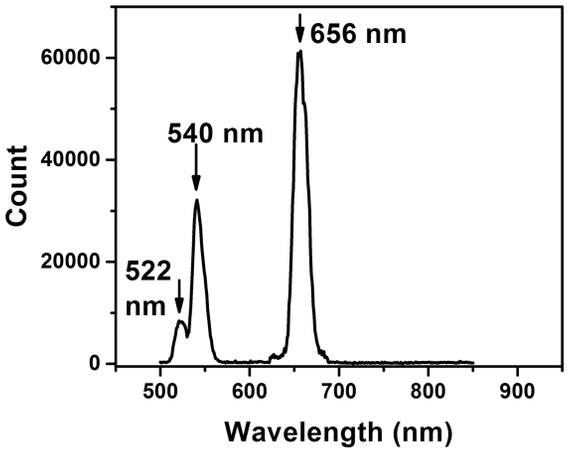

Figure 13. Spectrum of upconversion emission of the PMMA nano-composite film with $NaYF_4$: Yb^{3+}, Er^{3+} and AZO additives excited with a 980-nm laser diode.

The reason for the nano-composite film having an order of magnitude weaker upconversion fluorescence than that of the bulk phosphor powder, besides a limited concentration of the phosphor nanoparticles in the polymer host, could be related to the size effect. Based on the doping rate of the RE ions in the phosphor (see Sub-Section 2.2.2.1) and the computational approach in [70], the average number of the Er^{3+} and Yb^{3+} ions in the particles of an average diameter of 10 nm could be estimated as 128 and 628, respectively. The particles of 100-nm and 1-μm diameter would contain 10^3 and 10^6 times more RE ions. The upconversion emission involved two types of RE ions with the Yb^{3+} ion acting as a captor of the pump IR photons that later excited the Er^{3+} ion through the energy transfer process involving two IR photons, but not one. The more the RE ions contained in a phosphor particle, the stronger the upconversion emission would be. Accordingly, the nano-composite film including the nanoparticles of the upconversion phosphor of the size not exceeding ~200 nm should expectedly have upconversion QE less than that of the bulk powder with significant presence of 1-μm and greater particles. Adding the nanoparticles of AZO compound to the polymer nano-composite film helped to partially compensate the drop of upconversion QE due to the plasmon enhancement of the local pump IR optical field. As an illustration of possible applications for upconversion fiber illuminators, **Figure 14** presents the photograph of the tip of a single-mode fiber coated

http://dx.doi.org/10.5772/64816

using the above-described MAPLE/PLD method with a nano-composite film of PMMA + $NaYF_4$: Yb^{3+}, Er^{3+} + AZO pumped with a 980-nm laser diode (125-mW power). The tip of the fiber illuminated the white back side of a business card with visible upconversion light. The picture was taken with an iPhone 6 digital camera at dimmed room light.

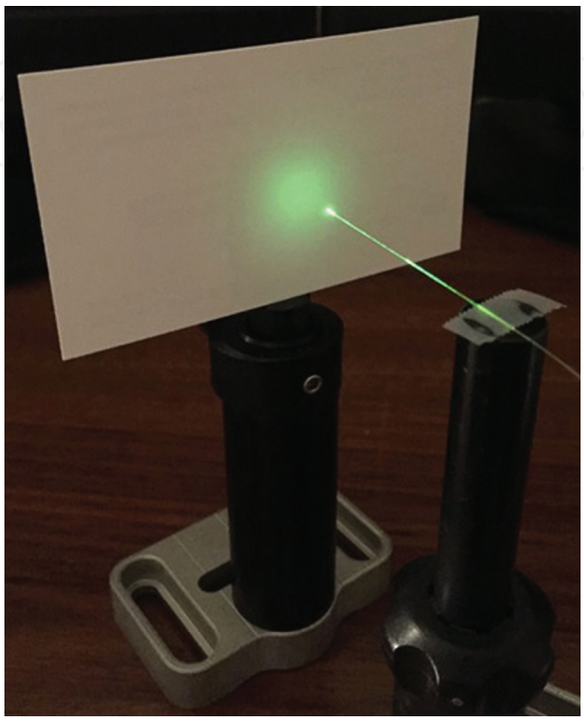

Figure 14. Photograph of the tip of a single-mode fiber coated with a nano-composite film of PMMA + $NaYF_4$: Yb^{3+}, Er^{3+} + AZO pumped with a 980-nm laser diode (125-mW power) illuminating white back side of a business card.

4. Conclusions

The multi-beam multi-target MAPLE/PLD method as a new variation of the film deposition via laser ablation makes possible to transfer concurrently several inorganic additives, such as an efficient upconversion RE inorganic phosphor and AZO compound, in nano-composite polymer films preserving crystalline structure of the additives and the upconversion emission properties. This is due to much better control of the deposition process of the materials of different nature from separate targets with different laser beams. The basic components of the new triple-beam triple-target MAPLE/PLD apparatus and the major process steps have been designed, built, and tested. The preliminary results indicated that adding AZO nanoparticles improved by a factor of 1.6 the upconversion quantum efficiency of the upconversion emission from the films possibly due to the plasmon enhancement of the local optical pump IR field in the vicinity of AZO nano-particles. The MBMT-MAPLE/PLD technique can find its applications in fabrication of multi-component polymer-inorganic composites with functionalities

spanning emitting light, sensing bio- and chemical agents, energy harvesting, and other applications.

Acknowledgements

The authors would like to acknowledge the support from DoD grants FA 9550-12-1-0068, W911NF-15-0446, W911NF-14-1-0093, W911NF-11-1-0192 and NSF HRD# 1002541 DU LS-LAMP grants.

Author details

Abdalla M. Darwish[1*], Sergey S. Sarkisov[2] and Darayas N. Patel[3]

*Address all correspondence to: adarwish@bellsouth.net

1 Dillard University, New Orleans, LA, USA

2 SSS Optical Technologies LLC, Huntsville, AL, USA

3 Oakwood University, Huntsville, AL, USA

References

[1] Dijkkamp D, Venkatesan T, Wu XD, Shareen SA, Jiswari N, Min-Lee YH, et al. Pulsed laser evaporation form high Tc bulk materials. Appl. Phys. Lett. 1987;5(8):619–621.

[2] Turner AF, Croft M. Vacuum deposited thin films using a ruby laser. Appl. Optics. 1965;4(1):147.

[3] Chrisey DB, Hubler GK. Pulsed laser deposition of thin films. New York: Wiley-Interscience; 1st edition. 1994, 648p.

[4] Scarfone C, Norton MG, Carter CB, Li J, Mayer JW. Characterization of $BaTiO_3$ thin films deposited by pulsed-laser ablation. In: Volume 201 - Proceedings of the 1990 MRS Fall Meeting – Symposium A - Surface Chemistry and Beam-Solid Interactions; 1990; Boston. New York: Cambridge University Press; 1991. p. 183.

[5] Fahler S, Stormer M, Krebs HU. Origin and avoidance of droplets during laser ablation of materials. Appl. Surf. Science. 1997;109/110:433.

[6] Kelly R, Rotenberg JE. Laser sputtering. Part III. The mechanism of sputtering of metals low energy densities. Nuclear Instrum. Methods Phys. Res. 1985;B7–8:755–763.

[7] Singh K, Narajan J. Pulsed-laser evaporation technique for deposition of thin films: physics and theoretical model. Phys. Rev. 1990;B41(5):8843.

[8] Holzapfel B, Roas B, Schultz L, Bauer P, Saemann-Ischenko G. Off-axis deposition of $YBa_2Cu_3O_{7-\delta}$ thin films. Appl. Phys. Lett. 1992;61(26):3178–3180. doi: 0003-6951/92/513178-03

[9] Gorbunov AA, Pompe W, Sewing A, Gaponov SV, Akhsakhalyan AD, Zabrodin IG, et al. Ultrathin film deposition by pulsed laser ablation using crossed beams. Appl. Surf. Sci. 1996;96–98:649–655.

[10] Guarniery CR, Roy RA, Saenger KL, Shivashnkar SA, Yee DS, Cuomo. Thin-film Bi-Sr-Ca-Cu-O high-temperature superconductors using pulsed laser evaporation from sintered disks. Appl. Phys. Lett. 1988;53(6):532–533. doi:0003-6951/88/320532-02

[11] Foster CM, Voss KF, Hagler TW, Mihailovich D, Heeger AJ, Eddy MM, et al. Infrared reflection of epitaxial $Ti_2Ba_2CaCu_2O_8$ thin films in the normal and superconducting states. Solid State Comm. 1990;76:651.

[12] Shinde SR, Ogale SB, Greene RL, Venkatesan T, Canfield PC, Budko SL, et al. Superconducting MgB2 thin films by pulsed laser deposition. Appl. Phys. Lett. 2001;79(2): 227–229.

[13] Fogarassy E, Fuchs C, Slaoui A, Stoquert JP. SiO2 thin-film deposition by excimer laser ablation from SiO target in oxygen atmosphere. Appl. Phys. Lett. 1990;57(7):664–666. doi:0003-6951/90/330664-03

[14] Balooch M, Tench RJ, Siekhaus WJ, Allen MJ, Connor AL, Olander DR, et al. Deposition of SiC films by pulsed excimer laser ablation. Appl. Phys. Lett. 1990;57(15):1540–1542. doi:0003-6951/90/411540-03

[15] Mihaiescu DE, Cristescu R, Dorcioman G, Popescu CE, Nita C, Socol G, et al. Functionalized magnetite silica thin films fabricated by MAPLE with antibiofilm properties. Biofabrication. 2013;5(1):015007.

[16] Paun IA, Moldovan AM, Luculescu C, Dinescu M. Antibacterial polymeric coatings grown by matrix assisted pulsed laser evaporation. Appl. Phys. A: Mater. Sci. Process. 2013;110(4):895–902.

[17] Shepard KB, Yunlong Guo, Arnold CB, Priestley RD. Nanostructured morphology of polymer films prepared by matrix assisted pulsed laser evaporation. Appl. Phys A: Mater Sci Process. 2013;110(4):771–7.

[18] Shepard KB, Priestley RD. MAPLE deposition of macromolecules. Macromol. Chem. Phys. 2013;214(8):862–72.

[19] Iordache S, Cristescu R, Popescu AC, Popescu CE, Dorcioman G, Mihailescu IN, et al. Functionalized porphyrin conjugate thin films deposited by matrix assisted pulsed laser evaporation. Appl. Surf. Sci. 2013;8:207–10.

[20] Singaravelu S, Mayo DC, Park HK, Schriver KE, Haglund RF Jr. Anti-reflective polymer-nanocomposite coatings fabricated by RIR-MAPLE. Proc. SPIE. 2013;8607:860718.

[21] Shepard KB, Arnold CB, Priestley RD. Origins of nanostructure in amorphous polymer coatings via matrix assisted pulsed laser evaporation. Appl. Phys. Lett. 2013;103(12): 123105.

[22] Caricato AP, Arima V, Cesaria M, Martino M, Tunno T, Rinaldi R, et al. Solvent-related effects in MAPLE mechanism. Appl. Phys. B: Lasers Optics. 2013;113(3):463–71.

[23] Birjega R, Matei A, Mitu B, Ionita MD, Filipescu M, Stokker-Cheregi F, et al. Layered double hydroxides/polymer thin films grown by matrix assisted pulsed laser evaporation. Thin Solid Films. 2013;543:63–8.

[24] McCormick RD, Cline ED, Chadha AS, Zhou W, Stiff-Roberts AD. Tuning the refractive index of homopolymer blends by controlling nanoscale domain size via RIR-MAPLE deposition. Macromol. Chem. Phys. 2013;214(23):2643–50.

[25] Canulescu S, Schou J, Fester S, Hansen KV, Conseil H. Deposition of matrix-free fullerene films with improved morphology by matrix-assisted pulsed laser evaporation (MAPLE). Chem. Phys. Lett. 2013;588:119–23.

[26] Visan A, Grossin D, Stefan N, Duta L, Miroiu FM, Stan GE, et al. Biomimetic nanocrystalline apatite coatings synthesized by Matrix assisted pulsed laser evaporation for medical applications. Mat. Sci. Eng.: B (Advanced Functional Solid-State Materials). 2014;181:56–63.

[27] Stokker-Cheregi F, Matei A, Dinescu M, Secu CE, Secu M. Photoluminescence of Eu-doped $LiYF_4$ thin films grown by pulsed laser deposition and matrix-assisted pulsed laser evaporation. J. Phys. D: Appl. Phys. 2014;47(4):045304.

[28] Constantinescu C, Matei A, Ion V, Mitu B, Ionita I, Dinescu M, et al. Ferrocene carboxaldehyde thin films grown by matrix-assisted pulsed laser evaporation for nonlinear optical applications. Appl. Surf. Sci. 2014;302:83–6.

[29] Palla-Papavlu A, Rusen L, Dinca V, Filipescu M, Lippert T, Dinescu M. Characterization of ethylcellulose and hydroxypropyl methylcellulose thin films deposited by matrix-assisted pulsed laser evaporation. Appl. Surf. Sci. 2014;302:87–91.

[30] Grumezescu V, Socol G, Grumezescu AM, Holban AM, Ficai A, Bleotu C, et al. Functionalized antibiofilm thin coatings based on PLA-PVA microspheres loaded with usnic acid natural compounds fabricated by MAPLE. Appl. Surf. Sci. 2014;302:262–7.

[31] Rusen L, Dinca V, Mitu B, Mustaciosu C, Dinescu M. Temperature responsive functional polymeric thin films obtained by matrix assisted pulsed laser evaporation for cells attachment-detachment study. Appl. Surf. Sci. 2014;302:134–40.

[32] Caricato AP, Arima V, Catalano M, Cesaria M, Cozzoli PD, Martino M, et al. MAPLE deposition of nanomaterials. Appl. Surf. 2014;302:92–8.

[33] Socol M, Preda N, Vacareanu L, Grigoras M, Socol G, Mihailescu IN, et al. Organic heterostructures based on arylenevinylene oligomers deposited by MAPLE. Appl. Surf. Sci. 2014;302:216–22.

[34] Constantinescu C, Matei A, Ionita I, Ion V, Marascu V, Dinescu M, et al. Azo-derivatives thin films grown by matrix-assisted pulsed laser evaporation for non-linear optical applications. Appl. Surf. Sci. 2014;302:69–73.

[35] Grumezescu V, Holban AM, Grumezescu AM, Socol G, Ficai A, Vasile BS, et al. Usnic acid-loaded biocompatible magnetic PLGA-PVA microsphere thin films fabricated by MAPLE with increased resistance to staphylococcal colonization. Biofabrication. 2014;6(3):035002.

[36] Sima F, Axente E, Iordache I, Luculescu C, Gallet O, Anselme K, et al. Combinatorial matrix assisted pulsed laser evaporation of a biodegradable polymer and fibronectin for protein immobilization and controlled release. Appl. Surf. Sci. 2014;306:75–9.

[37] Grumezescu V, Holban AM, Iordache F, Socol G, Mogosanu GD, Grumezescu V, et al. MAPLE fabricated magnetite-eugenol and (3-hidroxybutyric acid-co-3-hidroxyvaleric acid)-polyvinyl alcohol microspheres coated surfaces with anti-microbial properties. Appl. Surf. Sci. 2014;306:16–22.

[38] Axente E, Sima F, Sima LE, Erginer M, Eroglu MS, Serban N, et al. Combinatorial MAPLE gradient thin film assemblies signaling to human osteoblasts. Biofabrication. 2014;6(3):035010.

[39] Dinca V, Florian PE, Sima LE, Rusen L, Constantinescu C, Evans RW, et al. MAPLE-based method to obtain biodegradable hybrid polymeric thin films with embedded antitumoral agents. Biomed. Microdevices. 2014;16(1):11–21.

[40] Wangyao Ge, Qian Yu, Lopez GP, Stiff-Roberts AD. Antimicrobial oligo(p-phenylene-ethynylene) film deposited by resonant infrared matrix-assisted pulsed laser evaporation. Colloids and Surf B: Biointerfaces. 2014;116:786–92.

[41] Aronne A, Ausanio G, Bloisi F, Calabria R, Califano V, Fanelli E, et al. Structural characterization of MAPLE deposited lipase biofilm. Appl. Surf. Sci. 2014;320:524–30.

[42] Califano V, Bloisi F, Aronne A, Federici S, Nasti L, Depero LE, et al. Biosensor applications of MAPLE deposited lipase. Biosensors. 2014;4(4):329–39.

[43] Qian Yu, Wangyao Ge, Atewologun A, Lopez GP, Stiff-Roberts AD. RIR-MAPLE deposition of multifunctional films combining biocidal and fouling release properties. J. Mat. Chem. B. 2014;2(27):4371–8.

[44] Constantinescu C, Rotaru A, Nedelcea A, Dinescu M. Thermal behavior and matrix-assisted pulsed laser evaporation deposition of functional polymeric materials thin films with potential use in optoelectronics. Mat. Sci. Semicond. Process. 2015;30:242–9.

[45] Caricato AP, Cesaria M, Leo C, Mazzeo M, Genco A, Carallo S, et al. Very low roughness MAPLE-deposited films of a light emitting polymer: an alternative to spin coating. J. Phys. D: Appl. Phys. 2015;48(13):135501.

[46] Aronne A, Bloisi F, Calabria R, Califano V, Depero LE, Fanelli E, et al. Lipase biofilm deposited by matrix assisted pulsed laser evaporation technique. Appl. Surf. Sci. 2015;336:196–9.

[47] Iordache F, Grumezescu V, Grumezescu AM, Curutiu C, Ditu LM, Socol M, et al. Gamma-cyclodextrin/usnic acid thin film fabricated by MAPLE for improving the resistance of medical surfaces to Staphylococcus aureus colonization. Appl. Surf. Sci. 2015;336:407–12.

[48] Matei A, Constantinescu C, Mitu B, Filipescu M, Ion V, Ionita I, et al. Laser printing of azo-derivative thin films for non-linear optical applications. Appl. Surf. Sci. 2015;336:200–5.

[49] Stiff-Roberts AD, McCormick RD, Wangyao Ge. Material properties and applications of blended organic thin films with nanoscale domains deposited by RIR-MAPLE. Proc. SPIE. 2015;9350:935007.

[50] Grumezescu V, Andronescu E, Holban AM, Grumezescu AM, Socol G, Iordache F, et al. MAPLE fabrication of thin films based on kanamycin functionalized magnetite nanoparticles with anti-pathogenic properties. Appl. Surf. Sci. 2015;336:188–95.

[51] Caricato AP, Anni M, Cesaria M, Lattante S, Leggieri G, Leo C, et al. MAPLE-deposited PFO films: influence of the laser fluence and repetition rate on the film emission and morphology. Appl. Phys. B. Lasers Optics. 2015;19(3):453–61.

[52] Wangyao Ge, Atewologun A, Stiff-Roberts AD. Hybrid nanocomposite thin films deposited by emulsion-based resonant infrared matrix-assisted pulsed laser evaporation for photovoltaic applications. Org. Electron.: Mater. Phys. Chem. Appl. 2015;22:98–107.

[53] Janković A, Eraković S, Ristoscu C, Mihailescu N, Duta L, Visan A, et al. Structural and biological evaluation of lignin addition to simple and silver-doped hydroxyapatite thin films synthesized by matrix-assisted pulsed laser evaporation. J. Mater. Sci: Mater. Med. 2015;26(1):17.

[54] Paun IA, Acasandrei AM, Luculescu CR, Mustaciosu CC, Ion V, et al. MAPLE deposition of polypyrrole-based composite layers for bone regeneration. Appl. Surf. Sci. 2015;357:975–84.

[55] Darwish AM, Sagapolutele MT, Sarkisov S, Patel D, Hui D, Koplitz B. Double beam pulsed laser deposition of composite films of poly(methyl methacrylate) and rare earth fluoride upconversion phosphors. Compos Part B: Eng. 2013;55:139–46.

[56] Darwish AM, Wilson S, Sarkisov S, Patel D. Double pulse laser deposition of polymer nanocomposite $NaYF_4:Tm^{3+}$, Yb^{3+} films for optical sensors and light emitting applications. Proc. SPIE. 2014;8847:884702.

[57] Darwish AM, Burkett A, Blackwell A, Taylor K, Sarkisov S, Patel D, et al. Polymer-inorganic nano-composite thin film upconversion light emitters prepared by double-beam matrix assisted pulsed laser evaporation (DB-MAPLE) method. Compos Part B: Eng. 2015;68:355–64.

[58] Darwish AM, Burkett A, Blackwell A, Taylor K, Walker V, Sarkisov S, et al. Efficient upconversion polymer-inorganic nanocomposite emitters prepared by the double beam matrix assisted pulsed laser evaporation (DB-MAPLE), Proc. SPIE. 2014;9200:92000C.

[59] Darwish AM, Wilson S, Blackwell A, Taylor K, Sarkisov SS, Patel DN, et al. Ammonia Sensor based on polymer-inorganic nano-composite thin film upconversion light emitter prepared by double-beam pulsed laser deposition. Am. J. Mater. Sci. 2015;5(3A): 8–15.

[60] Darwish AM, Wilson S, Blackwell A, Taylor K, Sarkisov S, Patel D, et al. Polymer-inorganic nanocomposite thin film emitters, optoelectronic chemical sensors, and energy harvesters produced by multiple-beam pulsed laser deposition. Proc. SPIE. 2015;9586:958602.

[61] Darwish AM, Wilson S, Blackwell A, Taylor K, Sarkisov S, Patel D, et al. Multi-beam pulsed laser deposition: new method of making nanocomposite coatings. Proc. SPIE. 2015;9586:958605.

[62] Darwish A, Sarkisov S. Multiple beam pulsed laser deposition of composite films, US Patent Application No. 14/158,567, Filed 1/17/2014, Publication No. US 2014/0227461 A1.

[63] Darwish A, Sarkisov S. Multiple beam pulsed laser deposition of composite films, US Patent Application No. 14/506,685, Filed 10/15/2014.

[64] Darwish A, Mele P, Sarkisov S. Nano-composite thermo-electric energy converter and fabrication method thereof. US Patent Application No. 14/853,674, Filed 9/14/2015.

[65] West PR, Ishii S, Naik GV, Emani NK, Shalaev VM, Boltasseva A. Searching for better plasmonic materials. Laser Photonics Rev. 2010;4(6):795–808.

[66] Kim Y, Lee W, Jung D-R, Kim J, Nam S, Kim H, et al. Optical and electronic properties of post-annealed ZnO:Al thin films. Appl. Phys. Lett. 2010;96(17):171902.

[67] Tong H, Deng Z, Liu Z, Huang C, Huang J, Lan H, et al. Effects of post-annealing on structural, optical and electrical properties of Aldoped ZnO thin films. Appl. Surf. Sci. 2011;257(11):4906–11.

[68] Lin J-Y, Zhong K-D, Lee P-T. Plasmonic behaviors of metallic AZO thin films and AZO nanodisk arrays. Opt. Express. 2016;24(5):5125.

[69] Boyer JCh, van Veggel FCJM. Absolute quantum yield measurements of colloidal $NaYF_4$: Er^{3+}, Yb^{3+} upconverting nanoparticles. Nanoscale. 2010;2:1417–19.

[70] Liu H, Xu CT, Dumlupinar G, Jensen OB, Andersen PE, Andersson-Engels S. Deep tissue optical imaging of upconverting nanoparticles enabled by exploiting higher intrinsic quantum yield through use of millisecond single pulse excitation with high peak power. Nanoscale. 2013;20(5):10034–40.